SAE AERO DESIGN WEST 2022

Technical Design Report

Team Name: **QUATLAS**

Team Number: **012**

School Name: **M. S. RAMAIAH INSTITUTE OF TECHNOLOGY**

Faculty Advisor: **GURURAJ LALAGI**

Team Members:

Captain: ANUBHAV VISHWAKARMA

PARTHA MERAVANIGE
VEDARTH RAGHATATE
SANJEEV NAVARATNA
ANANYA MURALIDHAR
SHREESHMA HEGDE
MUHAMMAD SAFWAAN
CHAITRA G P
RAKSHITH SALIAN
VIKRAM VAIDYA
ARYAN VAIDYA
BHARATH M B
DHRUV DANGE
ROHIN JOSHI

RAMAIAH
Institute of Technology

STATEMENT OF COMPLIANCE

Certification of Qualification

Team Name	QUATLAS	Team Number	012
School	M. S. Ramaiah Institute of Technology		
Faculty Advisor	Gururaj Lalagi		
Faculty Advisor's Email	gururajlalgi@msrit.edu		

Statement of Compliance

As faculty Adviser:

NL (Initial) I certify that the registered team members are enrolled in collegiate courses.

NL (Initial) I certify that this team has designed and constructed the radio-controlled aircraft in the past nine (9) months with the intention to use this aircraft in the **2022** SAE Aero Design competition, without direct assistance from professional engineers, R/C model experts, and/or related professionals.

NL (Initial) I certify that this year's Design Report has original content written by members of this year's team.

NL (Initial) I certify that all reused content have been properly referenced and is in compliance with the University's plagiarism and reuse policies.

NL (Initial) I certify that the team has used the Aero Design inspection checklist to inspect their aircraft before arrival at Technical Inspection and that the team will present this completed checklist, signed by the Faculty Advisor or Team Captain, to the inspectors before Technical Inspection begins.

Signature of Faculty Advisor — Date: 27th Feb 2022

Signature of Team Captain — Date: 27th Feb 2022

1. TABLE OF CONTENTS:

TABLE OF TABLES

TABLE OF FIGURES:

TABLE OF SYMBOLS AND ACRONYMS:

b- Wing Span	L_v – Vertical Moment Arm
S- Area of the Wing	C_L - Coefficient of Lift
M.A.C.- Mean Aerodynamic Chord	C_D – Coefficient of Drag
V_h- Horizontal tail volume coefficient	AR - Aspect Ratio
V_v - Vertical tail volume coefficient	AR_H - Aspect Ratio of Horizontal Stabilizer
S_h - Horizontal tail planform area	SM - Stability Margin
S_v - Vertical tail planform area	FOS – Factor of Safety
L_H- Horizontal Moment Arm	AoA - Angle of Attack (α)
c- Wing Chord	V_{Stall} - Velocity of Stall
x_{np} - Distance of Neutral Point	$C_{L_{max}}$ - Maximum Coefficient of Lift
W - Weight of the airplane	C_m - Pitching Moment
L- Lift Force	D - Drag Force
T- Thrust Force	g- Acceleration due to Gravity
$C_{D,0}$ - Zero Lift Drag Coefficient	V_o- Maneuvering Velocity
τ – Time Constant	V- Airspeed/ Cruise speed
ζ – Damping Ratio	ω_n – Natural Frequency
$C_{n\beta}$ – Directional Stability Derivative	$C_{l\beta}$ – Lateral Stability Derivative
$C_{n\delta r}$ - Yaw Control Derivative	$C_{m\delta e}$ – Elevator Control Power
$C_{l\delta a}$ - Roll Control Derivative	FOM – Figure of Merit

2. <u>Executive Summary:</u> Winning the SAE Aero Design West competition has been Team Quatlas' endeavour since its inception. In our first attempt, our airplane carried the highest payload ever carried by an Indian team & we have not looked back since. We finished 10th overall last year despite the difficulties faced due to the pandemic, & we intend to build upon that this year. Before the new design, we reviewed & analysed the shortfalls of our previous years' airplanes and conducted extensive crash analysis of other competing aircrafts as well, to identify their causes for failure so that we could account for them in our design. The report will outline the design process, overall performance analysis, testing & integration, and manufacturing processes we followed. The first step in our design was to analyse the scoring equation, following which we conducted static thrust tests with various motor & propeller combinations to determine the maximum thrust available within 1000 watts. The team then conducted a detailed flight score analysis between various potential configurations, selecting the bi-wing configuration. We plotted a constraint diagram with all the given constraints in the rulebook, selecting a design point with the highest score & feasibility while considering other constraints for a safe flight envelope of our aircraft. A new fuselage design was implemented, improving our empty weight fraction from 0.4 last year to 0.34 this year. The conceptual design consisted of trade studies for various designs and configurations of the various components of the airplane, through an extensive literature survey. One of the major design changes this year was the adoption of the Bi-Wing Configuration for the wing for which we found it necessary to implement a winglet to reduce the wingspan, optimizing the flight score. We selected the S1210 airfoil for the blended wing planforms and NACA 0012 for the conventional tail. By conducting a topology study, we eliminated unnecessary weight from the landing gear. The preliminary design consisted of sizing all the components, followed by the detailed design, which included the sizing of the bolts for the assembly. We designed a modular airplane that could be disassembled for easy transportation, manufacturing, and repair. The airplane features improvements over the previous year's designs, such as a shorter wingspan and a lower expected empty weigh fraction. Thorough structural & performance analyses of the airplane were carried out to ensure desired performance within safe limits.

3. Mission Statement:

- To optimize the aircraft design to maximize the flight score prioritizing the scoring equation.
- To fabricate a highly accurate & rigid air frame structure.
- To take off within 100 ft and execute a full stop landing within 400 ft, without consuming more than 1000 W of power.

4. Objectives: We defined the following objectives, keeping them in mind throughout the design phase

O1	To find the potential configuration which will maximize the flight score.
O2	Implementation of winglets which would help us reduce the wingspan.
O3	Selecting a motor and prop combination that can give a higher power loading within 1000W.
O4	Conduct thorough analysis to minimize the empty weight of the aircraft.
O5	To design an easily accessible cargo bay to ensure unloading within 60 seconds.
O6	To create a flexible schedule accounting for the possibility of a lockdown due to covid.
O7	To design rigid joints between various components so that they don't fail in-flight.
O8	Implement a new fuselage structure which would help us with the fast & precise fabrication of the airframe structure.
O9	To ensure that the airplane takes off within 100 ft and lands within 400 ft whilst not weighing more than 55 pounds.
O10	Strictly adhere to the budget allocated for the project.

Table 1:Team objectives

5. Understanding Risks: We listed the following risks based on past experiences and literature survey.

Risk	Definition	Mitigation method
Aircraft crash during flight round	Unable to control airplane which results in a crash and irreparable damage to structure	Modular structure design in order to help in case of a crash.
Exceeding the 100ft line during takeoff	Airplane unable to takeoff within 100 ft, thereby making the flight round invalid.	Conduction of extensive numerical analysis on ground roll during take off
Radio communication failure	Loss of communication between the transmitter and the receiver due to improper range or during banking of the aircraft	Selection of a transmitter with sufficient range and using a receiver with two orthogonally placed antennae
Excessive empty weight	Improperly analyzed airplane components resulting in higher empty weight	Conducting trade-off studies to select suitable materials capable of handling expected loads while keeping empty weight to a minimum
	Unable to complete fabrication of the	

Failure to finish on time	airplane before the competition because of restrictions due to Covid-19 preventing us from accessing the workspace.	Design airframe structures which enable faster fabrication
Addition of ballast	Addition of ballas to bring the CG to the desired location, thus increasing the empty weight.	Fabricating the tail section first and then designing the nose accordingly

Table 2: Risks & Mitigation Methods

6. Gantt chart:

To make sure all team operations were in sync and the project was completed within the deadline, we employed the use of a Gantt chart in view of O6 for the various tasks involved. They were divided into design, fabrication, report and presentation and the time for each was estimated and allotted based on our previous experiences, giving allowances in each task for possible interruptions due to the second wave of Covid-19. We updated the chart weekly and worked extra hours the following week itself to prevent tasks from piling on if we lagged behind. Figure 1 shows the updated Gantt chart according to the new schedule.

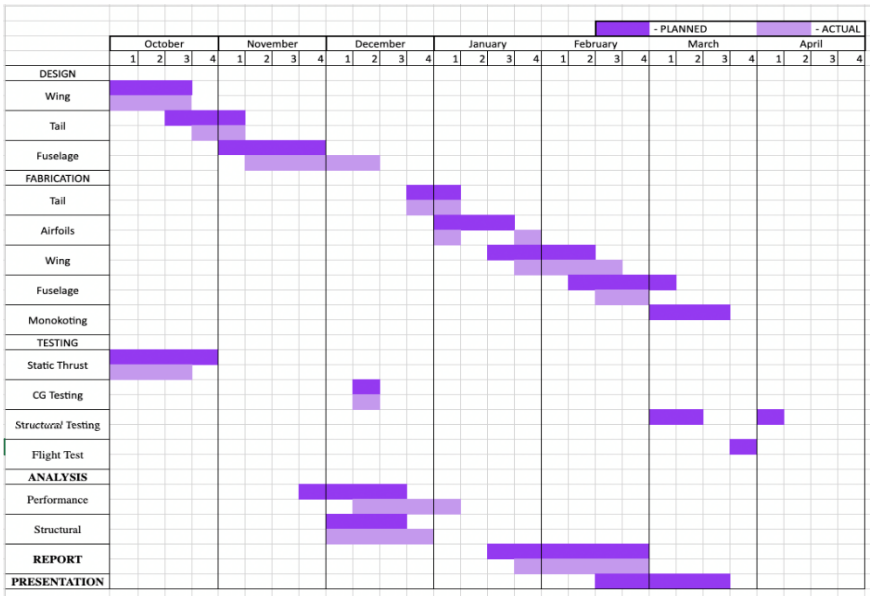

Figure 1: Gantt Chart

7. Conceptual Design:

7.1 Static Thrust Testing: We conducted the static thrust testing prior to the conceptual design to obtain the static thrust value needed for determining the gross weight from the constraint diagram. We compared the same motors as last year because of budget constraints.

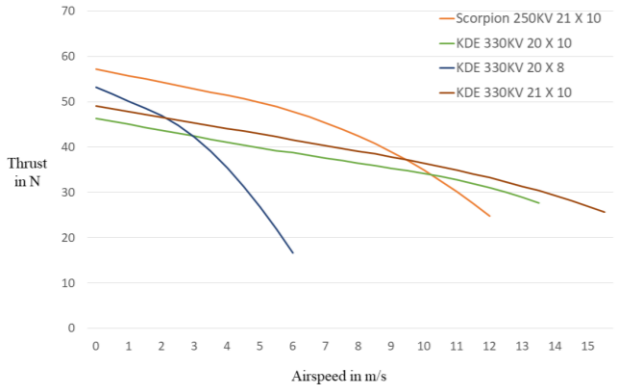

Figure 2: Thrust Lapse Characteristics

However, we tried different propeller combinations and tabulated their static thrust values. The below mentioned propellers were analyzed on Motocalc to get the thrust lapse of the propeller.

Motor	Propeller	Power Consumed (W)	Thrust (N)
T-Motor MN605S (320 KV)	19x8	936	49.80
	20x8	952	51.65
KDE5215F (330 KV)	**21x10**	**940**	**49.05**
	20x8	960	53.22
	20x10	980	46.30
Scorpion SII-4035-250KV	21x3.5	970	41.20
	22x12	1260	43.16

Table 3: Static Thrust Test Readings

7.2 Scoring equation analysis: The team analyzed the scoring equation and deduced the following parameters which were critical to optimizing the score of each flight round.

- Empty weight ratio – Lower the ratio, higher the payload lifted per flight round.
- Aerodynamic efficiency – Higher the efficiency, lower the thrust loading required to climb to the safe altitude thereby increasing the gross weight.
- Soccer ball configuration – Selecting the configuration which will have higher ratio of no. of soccer balls to length of cargo.
- Wing loading – Higher the wing loading, lower the wing area, resulting in lower wing span.
- Thrust loading – The lower the thrust loading is, higher the gross weight of the aircraft.
- Aspect Ratio – Lower the ratio, lower the wing span requiring a winglet to be designed to increase the aerodynamic efficiency or the effective Aspect ratio.

7.3 Configuration Selection: The team conducted a trade study based on low fidelity analysis to select the potential aircraft configuration to achieve O1. To fulfil this, we considered empty weight and wing span, without compromising the static and dynamic stability of the aircraft, ensuring a safe flight round. We evaluated the performance of each configuration on a scale of 1 to 5 with respect to the Figure of Merit.

Figure 3: 4 Identified Design Alternatives clockwise from top like Bi-plane, conventional, tandem wing & foreplane

FOM	Score factor	Bi-wing	Conventional	Fore Plane	Tandem Wing
Wing Span	5	**5**	2	3	4
Empty Weight	5	**0.5**	1	1	2
Stability	2	**3**	3	1	1
Total		**33.5**	21	22	32

Table 4: Weighted Pugh Matrix for the Considered Design Alternatives

The team considered lift distribution between wings and horizontal stabilizer to predict the wingspan of each configuration. To predict the empty weight of the aircraft, we analysed the weight of each configuration by considering the type of attachment, length of cargo and tail arm. We then calculated a score for each type of configuration, finalizing upon the bi-wing configuration as it gave the highest overall score owing to its weight sharing between the horizontal stabilizer and wing, allowing us to reduce the wing span or increase the weight of the aircraft (O1).

7.4 Constraint Diagram: The team found it best to generate the constraint diagram at the beginning of the design process as we were implementing a bi-wing configuration over the previous monoplane

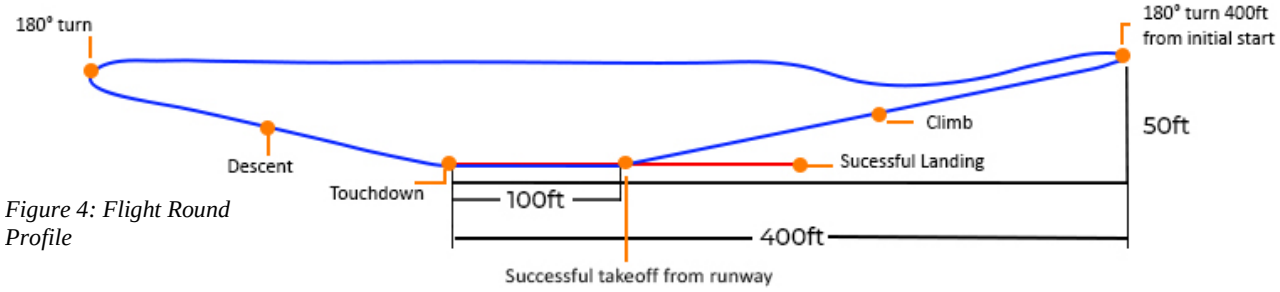

Figure 4: Flight Round Profile

configuration. The take-off equation (F1) was modified for which we assumed the area of the two wings as equal and stacked over each other with the C_L assumed to be the sum of the C_L's of each of the wings. This allowed us to opt for a higher wing loading. We considered the constraint of achieving an altitude of 50ft before the sustained level turn as the aircraft will lose altitude during the turn due to the loss of headwind. We found this loss in altitude to be approximately 30ft until the aircraft achieves its terminal velocity. To account for this, a 20ft allowance was given to avoid a crash. This constraint was imposed on

the thrust loading of the aircraft through the climb equation. We chose the flight path angle of 10° from last year's aircraft and iterated it through the design phase to obtain the aerodynamic efficiency which was later found to be 9.4. This gave us the climb curve where the thrust loading is 0.28. To obtain the wing loading, we considered typical cruise velocities around 39.37 – 42.65 ft/s as they gave us an allowance of at least 40 N of available thrust to manoeuvre the aircraft safely.

Velocity (ft/S)	Drag at cruise	Available Thrust
32.81	9.48	36
36.09	11.47	34
39.37	**13.654**	**31**
42.65	**16.025**	**30**
45.93	18.585	28
49.21	21.336	25

Table 5: Selection of Cruise Velocity

Using this velocity and the calculated bi-wing configuration's lift coefficient, the typical wing loading was found to be between 150-200 N/m^2. We found the Reynolds number to be approximately 500000 considering the chord to be 20". Following [3] we found the C_{fe} at Re 500,000 to be 0.003 and the $C_{D,0}$ was approximated as $4C_{fe}$ i.e. 0.012. We assumed an aspect ratio of 4 and Oswald's efficiency as 0.8 giving us a 13N drag during climb. We plotted the sustained level turn considering a bank angle of 60° giving us a load factor of 2. The take-off and landing curves correspond to the 100ft & 400ft take-off and landing distances respectively. The constraint diagram is shown above.

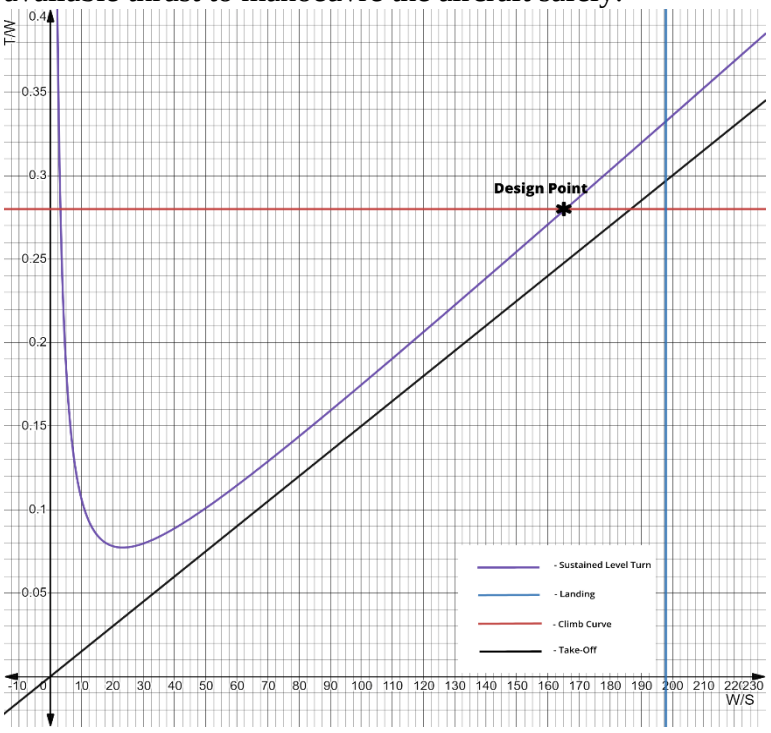

Figure 5: Constraint Diagram

Wing Loading	Take-off distance	Landing distance
160 N/m^2	82.00 ft	136.73 ft
165 N/m^2	**84.58 ft**	**144.10 ft**

Table 6: Selection of Wing Loading

7.5 <u>Selection of design point:</u> The thrust loading was found to be 0.28 from the climb curve. We found the weight from thrust loading considering the thrust and drag during climb.

We tabulated different take-off and landing distances giving an allowance of 15 feet to meet the competition requirements and chose the wing loading to be 165 N/m^2.

7.6 Payload weight: The effective thrust during take-off was calculated to be 35.56 N. We then found the gross weight as 27.99 lb. using the thrust loading corresponding to the design point. We reached an empty weight fraction of 0.4 last year hence, we targeted 0.36 this year after thoroughly analysing the previous structure and adopting a new structure design. This gave us a payload weight of 17.9 lb.

7.7 Trade Studies:

7.7.1 Empennage We considered different tail configurations such as H,T,V and conventional with the maximum score factor being given to the least weight in view as per O4. The T-tail & H-tail were both discarded as they require a stronger vertical & horizontal stabilizer respectively compared to the other configurations, increasing the total weight. Though the V-tail provides a lesser empty weight it was neglected as its complex design requires highly precise manufacturing to function effectively. We finalized the conventional tail due its manufacturability, reduced weight & good aerodynamic efficiency.

		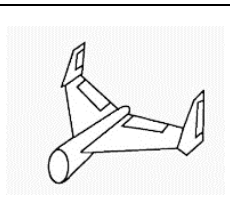	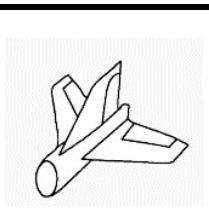	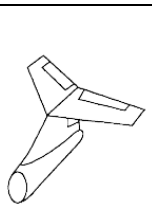	
FOM (Figure of Merit)	**Score Factor**	**H-tail**	**Conventional tail**	**T-tail**	**V-tail**
Performance	**2**	4	**5**	4	3
Stability& Control	**3**	3	**3**	1	2
Manufacturability	**4**	2	**5**	4	1
Least Weight	**5**	1	**4**	2	3
Total		30	**59**	37	31

Table 7: Tail Configuration

7.7.2 Wing planform: The team considered the elliptical, tapered, rectangular and blended wing configurations with the highest factor given to least weight accounting for O4. A score factor of 4 was given

to induced drag as a smaller aspect ratio was vital for a smaller wingspan (O2) and a factor of 3 was given to manufacturability as it was key to build the aircraft in a short time.

			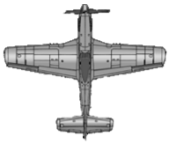		
FOM (Figure of Merit)	**Score Factor**	**Elliptical wing**	**Tapered wing**	**Rectangular wing**	Blended
Manufacturability	**3**	1	3	5	**4**
Least induced drag	**4**	5	4	1	**3**
Least weight	**5**	3	2	1	**3**
Total		38	35	24	**39**

Table 8: Wing Planform

7.7.3 Winglet: We compared the canted winglet, blended winglet and tip fence configurations based on their manufacturability, performance and weight. Again, the highest score factor was given for the least weight parameter. Hence, we rejected the tip fence in view of O4. We selected the canted winglet as the blended winglet was ruled out due to complexities in manufacturing.

				
FOM (Figure of Merit)	**Score Factor**	**Canted winglet**	**Blended winglet**	**Tip fence**
Manufacturability	**3**	**5**	3	4
Performance	**4**	**3**	4	2
Least weight	**5**	**4**	3	2
Total		**47**	40	30

Table 9: Winglet Configuration Selection

7.7.4 Landing Gear: We considered the tricycle and tail dragger configurations for the landing gear. We selected the tricycle configuration as it had a higher acceleration despite having a low C_L at the start of the ground roll whereas the tail dragger has poor ground manoeuvrability and stability.

		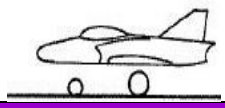	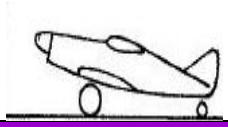
FOM (Figure of Merit)	**Score Factor**	**Tricycle**	**Tail dragger**
Ground maneuverability	**1**	**5**	1
Ground stability	**2**	**4**	3
Lower impact on landing	**3**	**4**	2
Manufacturability	**4**	**5**	1
Least weight	**5**	**3**	3
Total		**60**	32

Table 10: Landing Gear Configuration

8. Preliminary Design:

8.1 Calculation of spherical cargo and amount of regular boxed cargo: We calculated the wingspans using the obtained design point, calculated wing area, gross weight of the aircraft and the assumed aspect ratio of 4. We then found the length of the cargo by considering the lengths of the regular boxed cargo and the lengths of the different spherical cargo configurations. We used an assumed empty weight fraction to find the weight of the payload. Using this data, we obtained the final flight scores for each configuration.

				
FOM (Figure of Merit)	**Score Factor**	**1 Ball Configuration**	**Row Configuration**	**Stacked Configuration**
Manufacturability	**2**	**4**	5	1
Aerodynamic Efficiency	**3**	**5**	4	1
Least weight	**4**	**5**	4	3
Flight Score	**5**	**4**	3	5
Total		**63**	53	42

Table 11: Soccer Ball Configuration

We considered the 1 ball, 2 ball in a stack and 2 in a row (along the fuselage of the aircraft) soccer ball configurations. We did not consider any 3 ball configurations as they would lead to higher drag and a

higher empty weight than the 2 ball configurations. We used a weighted Pugh matrix for selecting the configuration of this year's airplane. Each figure of merit (FOM) was evaluated based on their importance with the maximum score factor corresponding to 5, with a minimum of 1. The performance of each configuration was evaluated on a scale of 1 to 5 as well with respect to the figure of merit (FOM).

We rejected the stacked configuration despite it giving a higher FS as it would result in a higher drag and would be difficult to manufacture. Although the row configuration would have simplified CG balancing by having its cargo bay being symmetric about C.G, we finalized upon the 1 ball configuration as the C.G would be balanced by keeping the ball in the designated spherical cargo bay position while conducting the C.G balance test and the regular boxed cargo would be symmetrical about the C.G.

8.2 Airfoil analysis: The team considered different airfoils which had a relatively higher C_{Lmax} in view of O9. We compared the E423, CH10, S1223, S1210 & fx74cl5140 for the wings. We discarded S1223, fx74Cl5140 as they have a significantly lower value of C_L/C_D than the rest, finalizing upon the S1210 for the wings as it had the highest value of C_{Lmax} & stalls at a higher angle than E423 & CH10.

We required positive lift from the horizontal stabilizer, hence, the team considered airfoils such as NACA 2411, NACA 2412 and NACA 0012. Although NACA 2411 & 2412 provided lift at zero AoA, they were discarded due to their negative pitching moment about their aerodynamic centre. This would have complicated the positioning of C.G at an appropriate position of M.A.C, creating difficulty in obtaining the SM. Hence, we selected NACA 0012 for the empennage due to its proven performance and efficiency.

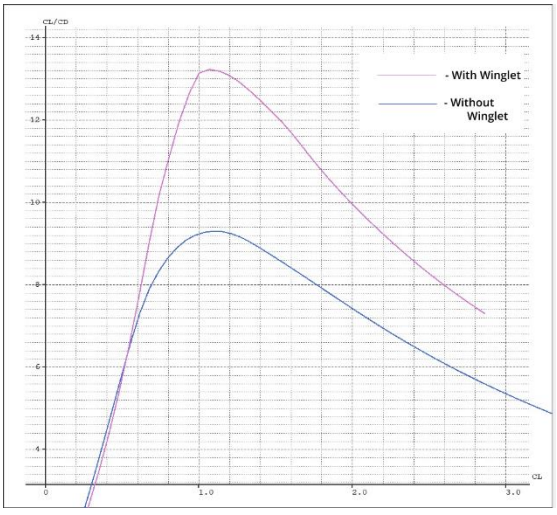

Figure 6: L/D v/s C_L comparison

8.3 Wing Design: We found the wing area to be 1164.1 in^2 by fixing the wing loading as 165 N/m^2 from the design point.

8.3.1 Winglet Design: We found through a literature survey for various winglet configurations, that the sweep angle should be in the range of 45-60^o with the winglet span being 15-20% of the wing span. An XFLR5 analysis

for this range of values revealed a sweep angle of 60° with a winglet-span equal to 10% of the wingspan provided maximum aerodynamic efficiency. With this combination, we conducted a CFD analysis on the following winglet shapes finalizing shape 1 as it had the highest aerodynamic efficiency.

Winglet shapes	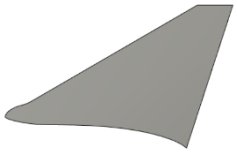 1	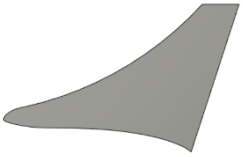 2	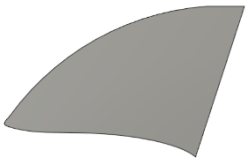 3
L/D	**13.2**	9.156	11.96

Table 12: Winglet Comparison

8.3.2 Aspect Ratio (AR): The team observed that increasing the AR would increase the wingspan, going against O2 and minimizing our flight score. Hence, we opted for a winglet design which increased the effective AR whilst maintaining a smaller wingspan. The wing design process was started by referencing existing competition aircrafts and their aerodynamic efficiencies without winglets. We then calculated the respective AR's (F3) inputting maximum aerodynamic efficiency from 8 to 12. We assumed Oswald's efficiency to be 0.8 and the skin friction coefficient as 0.03. We then found the maximum aerodynamic efficiencies of the wing with the winglet for each of the obtained AR'S through XFLR5, calculating the effective AR'S from them. Finally, we selected an AR of 3.86 without winglets as this gave us the required aerodynamic efficiency of 9.4 during climb with winglets, allowing us to achieve the 50ft altitude required to safely perform the sustained level turn.

Max Aerodynamic efficiency	Aspect Ratio	Max Aerodynamic efficiency (with winglet)	Effective Aspect Ratio
8	3.06	11.79	5.9
9	**3.86**	**13.02**	**7.2**
10	4.77	13.81	8.1
11	5.77	14.88	9.4
12	6.86	16.244	11.2

Table 13: Selection of Aspect Ratio

8.3.3 Wing Sizing: We selected the blended wing configuration as discussed earlier. We then evaluated wings of different root chords with the taper ratio 0.5. Upon iterative analysis on MATLAB, we established the span of each side wing as 20.376" & mid wing span as 25.747" considering aerodynamic

efficiency, weight and induced drag. Finally, we obtained the root chord, tip chord and MAC as 20.6692", 10.33" and 17.423" respectively.

8.4 Sizing and Static stability:

8.4.1 Horizontal stabilizer: The team decided to provide positive lift from the horizontal stabilizer in view of increasing the payload capacity of the plane. To implement this, we offset the C.G towards the tail from the aerodynamic centre, creating the pitch up moment which is countered by the positive lift from the horizontal stabilizer through the positive tail setting angle provided to it. We established a static margin of 0.1 as it provided good static & dynamic stability based on a thorough literature survey and the team's prior successful flights. We maintained the horizontal tail volume ratio at 0.65 based on our previous experiences and selected the tail arm's length as 45.44" as it provided sufficient static stability while keeping empty weight minimal. We then calculated the horizontal area through an iterative process as 0.42 times the wing area giving us 974.33 in^2, V_H as 0.65", b_H as 40.0319", C_r as 20.167", C_t as 10.0813", MAC as 15.0813" and AR_H as 2.647 being finalized. We generated the following curve between C_m vs C_L. The slope was found to be -0.1, ensuring SM of 0.1 which was desirable as it ensured good static and dynamic stability known to us through our past experiences and a literature review. We provided a wing setting angle of 5^o as it provided the highest aerodynamic efficiency to the airfoil as per XFLR5 analysis. The above-mentioned values along with the C.G position and tail setting angle were iterated until a static margin of 0.1 was maintained. Finally, the C.G was finalized at 37% of M.A.C.

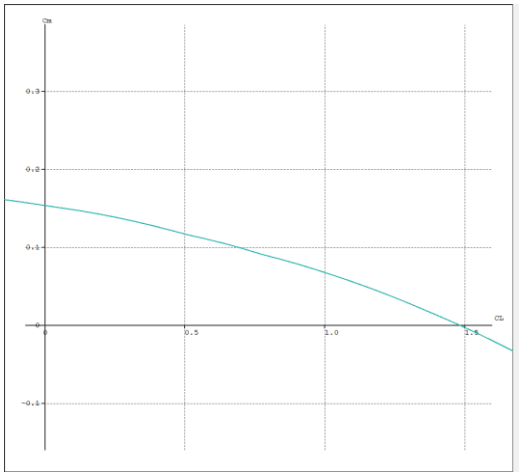

Figure 7: C_m vs C_l for horizontal stabilizer

8.4.2 Vertical Stabilizer: We sized the vertical stabilizer keeping in mind yaw and lateral stability. Receiving lateral stability from the vertical stabilizer was crucial as we did not give a dihedral in the wing to provide lateral stability. We iterated the vertical stabilizer sizing to get $C_{l\beta}$ & $C_{n\beta}$ negative & positive respectively. After multiple iterations, we finalized S_v at 325.948 in^2, tip chord of 10.139", root chord of

20.27", M.A.C. of 19.7" with a span of 21.437". The static stability in yaw & lateral mode of the finalized vertical stabilizer is shown above from which $C_{l\beta}$ & $C_{n\beta}$ were -0.0128/rad & 0.3406/rad respectively.

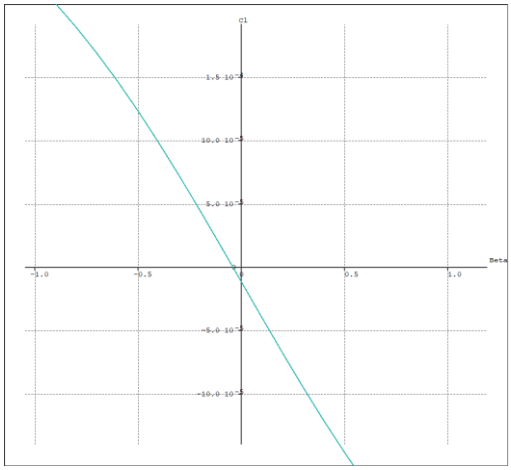

Figure 8: C_l v/s β

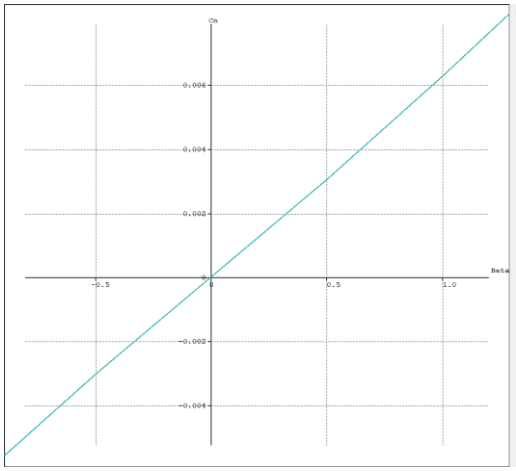

Figure 9: C_n v/s β curve

8.5 Dynamic Stability:

Mode	Level 1 Flying Quality Requirement	Stability Characteristics for Fully Loaded Case	Flying Quality Level Achieved
Short Period Mode	$0.35 < \zeta_{sp} < 1.30$	$\zeta_{sp} = 0.93138$	Level 1
Phugoid Mode	$\zeta > 0.04$	$\zeta = 0.116$	Level 1
Roll Mode	$\tau < 1.0$ s	$\tau = 0.0826$ s	Level 1
Dutch Roll Mode	$\zeta > 0.08$	$\zeta = 0.92$	Level 1
	$\zeta\omega_n > 0.15$ rad/s	$\zeta\omega_n = 2.098$ rad/s	Level 1
	$\omega_n > 1.0$ rad/s	$\omega_n = 2.28$ rad/s	Level 1
Spiral Mode	$T_2 > 20$ s	$T_2 = 66.67$ s	Level 1

Table 14: Aircraft Flying Qualities

We used inertial properties from the CAD file for the fully loaded aircraft to define the inertia in XFLR5, giving the eigen values used to find the damping ratio, natural frequency & the time taken to double the amplitude. This enabled us to predict & tabulate the flying quality of our aircraft. All the modes were found to be dynamically stable & qualified for level 1 flying quality except spiral mode however, the time to double its amplitude was 66.67 sec, thus qualifying for level 1 flying quality.

8.6 Downwash & Upwash:

We determined the positions of the top wing and the horizontal stabilizer using XFLR5. The goal was to place the horizontal stabilizer at a location

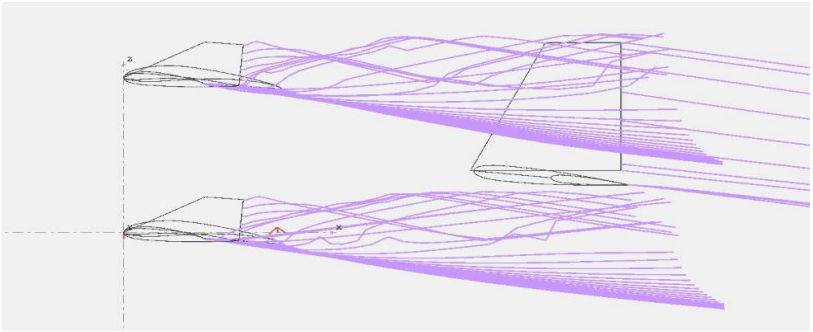

Figure 10: Downwash & Upwash Effect on Horizontal Stabilizer

where it did not experience any downwash from the top wing or upwash from the bottom wing. As the position of the bottom wing was fixed, we altered the height at which the top wing should be place to obtain an ideal position for the horizontal stabilizer. From the image shown below we can observe that the horizontal stabilizer is unbothered by the downwash or upwash caused by the wings. We obtained the height of the top wing to be at 24" from the lower wing & we obtained the height of the horizontal stabilizer from the lower wing to be 10".

8.7 Control Surface and servo Sizing: We designed the elevator such that its effectiveness is equal to 0.5 due to its proven performance for us in previous flights. The parameters corresponding to the elevator are tabulated below. The calculated values for the maximum torque experienced by the control surface were validated through XFLR5 analysis. For all the servo sizing we referred to (F2). We finalized the Hitec HS-225MG as its rating is higher than the maximum torque experienced by the elevator.

The rudder area was greater than that of our previous aircrafts as it will also be used to provide yaw control, roll control, and spin recovery to the aircraft. We opted to use a ratio of 0.4 whose parameters are tabulated below, finalizing upon the Hitec HS-225 MG as its rating was higher than the maximum torque experienced by the rudder. The team decided to employ flaperons as they increased the lift coefficient during take-off thereby reducing the take-off length. We followed the design process as given in [5] and finalized the aileron effectiveness parameter at 0.6. The data corresponding to this effectiveness was tabulated with the team finalizing upon Hitec HS-645 MG.

Control Surface	Control surface/Surface Area	Area(in^2)	Derivative (rad^{-1})	Deflection Range	Torque(OZ-in)	Selected Servo
Elevator	S_e/S_H=0.25	151.330	$C_{m_{\delta e}}$ = -0.949	±25°	45.74	Hitec HS-225 MG (max Torque 67oz-in)
Rudder	S_r/S_V=0.4	130.3792	$C_{n_{\delta r}}$ = -0.06704	±30°	56.6448	Hitec HS-225 MG
Flaperon	S_a/S=0.282	1641.12025	$C_{l_{\delta a}}$ = 0.0046122	±30°	110.457	Hitec HS-645 MG (Max torque 133 oz-in)

Table 15: Servo Sizing & Control Derivatives

8.8 Landing Gear Sizing: The team decided a propeller clearance of 3" to be sufficient. We finalized the We finalized the landing gear height at 7.25" after we found the minimum required height of the landing gear to be 6.8". We adopted the tri-cycle landing gear with the main landing gear positioned 1.5" aft of C.G. We secured the nose gear to the fuselage 15" from the C.G reducing the load experienced by it to only 14.65% of the total load distribution. We determined the wheel track to be 18" after choosing an overturn angle of 30°.

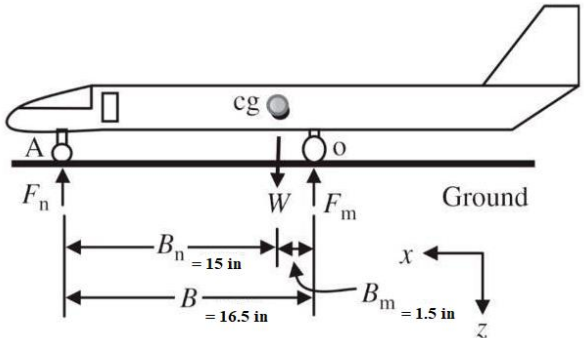

Figure 11: Landing Gear Sizing

9. Detailed Design:

9.1 Fuselage: The fuselage was designed keeping in mind O5 & O8. We opted for a stringer-frame structure consisting of 8 pre laser cut guide ways of balsa & aero-ply passing through cross-sections to accelerate fabrication and ensure structural rigidity. This structure enabled us to completely fabricate the fuselage in under a week. Cross sections were cut from 0.118" aero-ply sheets with their shapes being derived keeping in mind cargo unloading, directional stability & drag. Non-critical areas were removed to reduce weight.

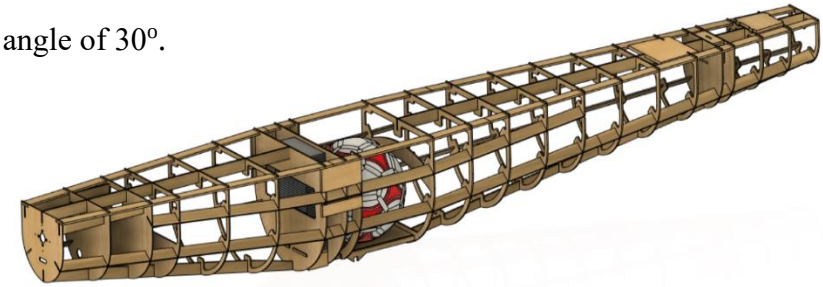

Figure 12: Fuselage & Cargo Bay Design

9.2 Cargo Bay Design: The cargo bay carries 1 football and has 1 separate compartment to house the regular boxed cargo. This compartment holds 16 lbs. of regular boxed cargo and is symmetric about the C.G, keeping the variation of empty C.G and fully loaded C.G to within an inch.

9.3 Wing: We laid out S1210 airfoils onto an aluminum spar, the major load bearing member. A truss was made in the airfoil sections to withstand the wing load while having minimal weight. We passed multiple

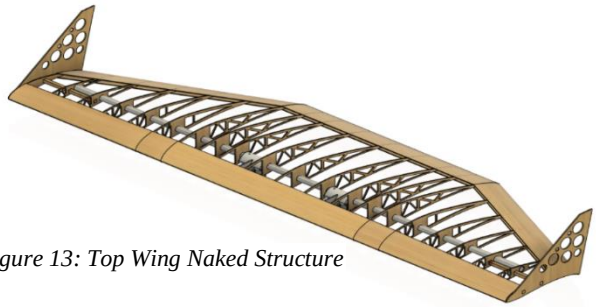

Figure 13: Top Wing Naked Structure

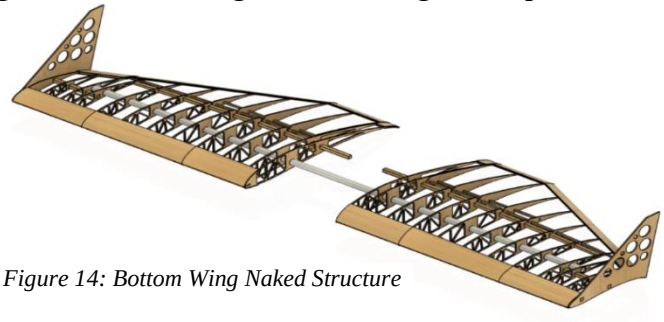

Figure 14: Bottom Wing Naked Structure

secondary spars through them to increase the wings' strength and maintain their alignment.

9.4 Horizontal & Vertical Stabilizer: Both stabilizers have truss structured airfoils like the wing made of balsa, except for those used for attachments, which are of plywood. They hold spars at the rear end to ensure alignment and strength but the vertical stabilizer has an additional vertical spar, restricting its movement about the X axis.

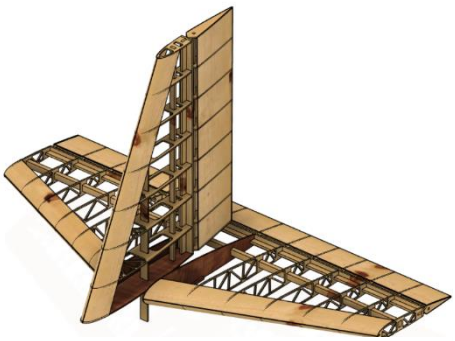

Figure 15: Empennage Naked Structure

9.5 Attachments & Assembly: Several rigid attachments were designed & fabricated to provide modularity for the aircraft while keeping O7 in mind.

9.5.1 Wing Attachments:

Hard balsa was used to connect the top wing to the fuselage. A 3D printed ABS plastic attachment connects the top wing with hard balsa, which in turn is connected with the fuselage on basswood plates through 0.236" bolts. The bottom wing is connected with the fuselage through 0.314" bolts after placing it on 2 balsa blocks.

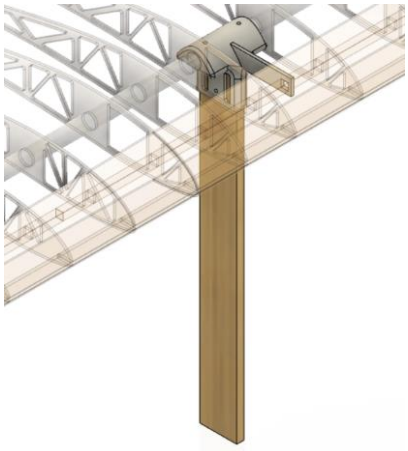

Figure 16: Top Wing Attachment

Figure 17: Bottom Wing Attachment

9.5.2 Tail Attachments: Basswood plates are used to connect the horizontal stabilizer to the fuselage. Balsa blocks stuck onto the vertical stabilizer are bolted onto the same plates using 0.196" bolts. As shown in fig 18, we restricted the stabilizers movement about X axis by compiling balsa sheets into a block.

9.5.3 Wing Setting Angle: Multiple custom attachments are made to ensure AoA of both the wings. For the lower wing, a 0.197" balsa sheet was laser cut and fit between two cross-sections of the fuselage. A secondary spar rests on this sheet. For the top wing, the 3D print attachment was given an extension through which a secondary spar passes through, ensuring our required wing setting angle of 5°.

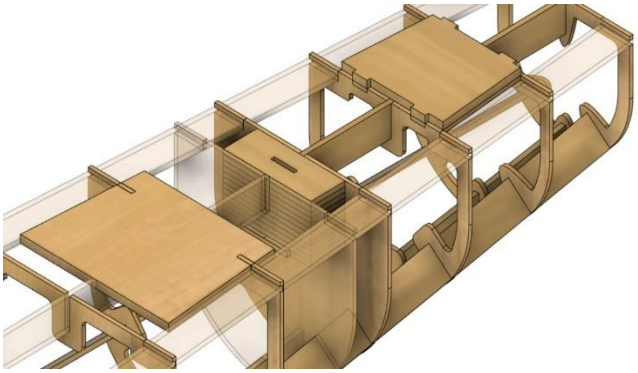

Figure 18: Tail Attachments on Fuselage

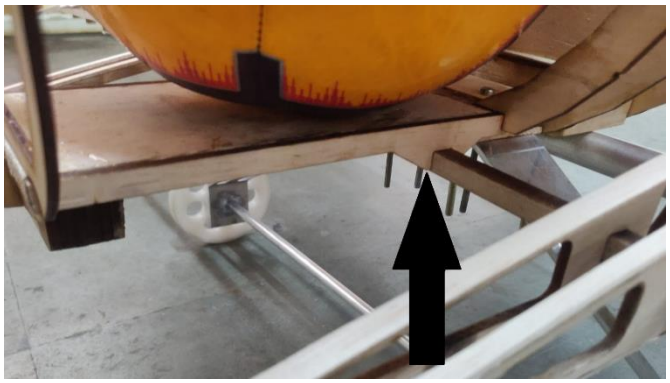

Figure 19: Bottom Wing - Wing Setting Angle Attachment

10. Analysis:

10.1 Tools used:

Tools	Description
Numerical analysis	MATLAB was used to predict the takeoff and climb performance.
Aerodynamics	We relied on XFLR5 as we lacked wind tunnel, for CFD Autodesk CFD was used
Simulation	Autodesk Fusion 360 was used for stress FEA
2D drawing	We used Autodesk Inventor for obtaining the standard 3-view orthographic projection of the airplane in the 2D drawing.
FEM	We used ANSYS to conduct analysis on non-linear materials used in the airplane.
Powerplant analysis	We used Motocalc to determine the most suitable motor- propeller combination.

Table 16: Analysis Tools Used

10.2 Performance Analysis:

10.2.1 Take-off: As there was a constraint of 100 ft on the take-off distance, the team found it essential to accurately predict the take-off distance so as to not render our flight rounds invalid. We ran a numerical analysis on MATLAB, giving us the take-off length as 88.58 ft and take-off velocity as 33.717 ft/sec. The flare distance was found to be 30.13 ft.

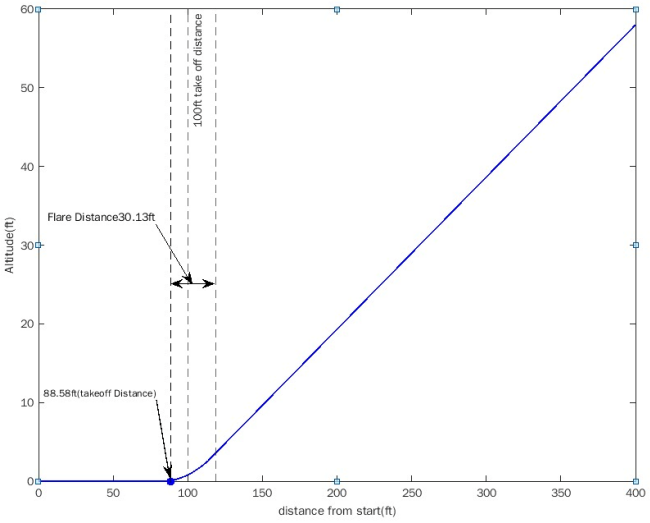

Figure 20: Take-off & Climb Performance

10.2.2 Climb: We found the climb angle to be 9.995^{o}, with the velocity during steady climb as 35.911 ft/sec. We calculated the altitude attained before climb to be 58 ft which was above the calculated safe altitude required before starting the sustained level turn.

10.2.3 Maneuver: We calculated the minimum radius of turn to be 49.08 ft with a bank angle of 60^{o} as the constraint after considering the Apollo 11 airfield which does not have any obstacles restricting the coordinated turn. To execute this manoeuvre, the aircraft will fly at a minimum speed of 38.6811 ft/s.

10.2.4 Cruise: We found the cruise velocity to be 41.0357 ft/sec from the selected wing loading of the aircraft, C_L at wing and tail setting angle of 1.753^{o}

10.2.5 Landing: The touch down velocity was calculated as 31.46 ft/s with the landing ground roll to be 146.03 ft, well within the limit of 400 ft as given in the rulebook.

10.3 Dynamic Thrust Analysis: We obtained dynamic thrust values at different air speeds using Motocalc as the team did not have access to a wind tunnel. We input this data into MATLAB to obtain a plot of available thrust to velocity. We found the thrust generated during cruise velocity to be excess of 18 N allowing the aircraft to perform the required maneuver hence, validating the design. The drag corresponding to the landing gear & fuselage was found through empirical formula & added to the drag generated through the wing & tail.

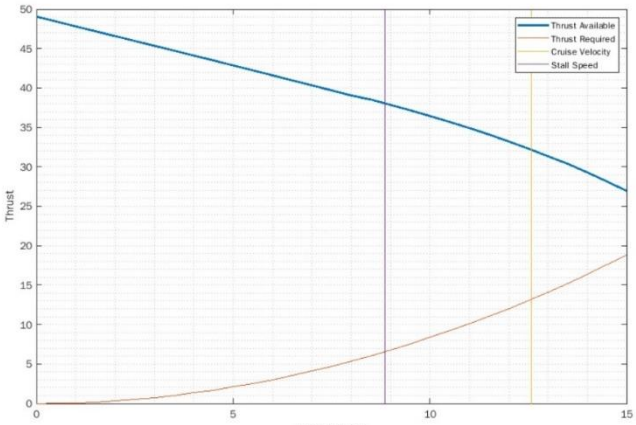

Figure 21: Dynamic Thrust

10.4 Payload prediction: We found the density altitude at Apollo XI Flying Field averaged roughly 1000 ft between April 8th and April 10th. We converted the thrust, drag and lift into functions of density for generating the TDS and computed the range of density altitudes for which the predicted payload could be lifted to lie between -500 ft and 5000 ft, with a step increase of 500 ft. We plotted these points between density altitude (ft) and payload (lb) and used regression to find the straight line of best fit through the points. We obtained the slope of this line as - 0.00097.

10.6 Structural Analysis:

10.6.1 V-n Diagram: We generated a V-n diagram for all the aircraft components and determined their corner velocities. We obtained the minimum corner velocity for the wing as 79.417ft/s and considered it as the corner velocity for the entire aircraft.

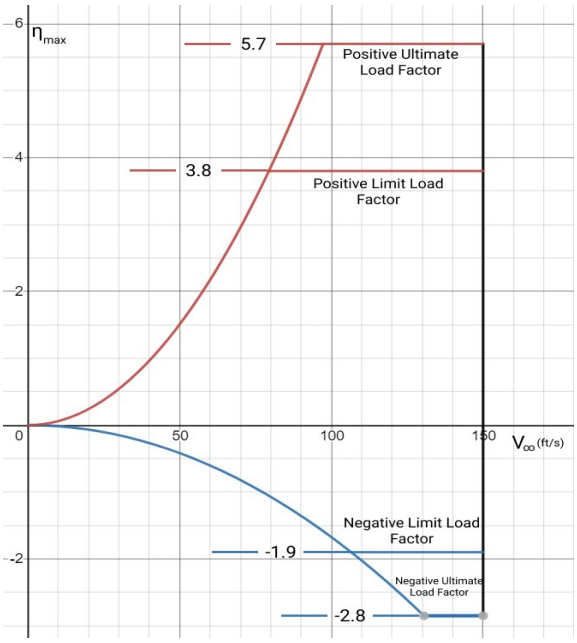

Figure22: V-n Diagram

10.6.2 Design & Ultimate Loads:

Wing Spar: The wing experienced the maximum load during maneuver at a bank angle of 60°. This corresponded to a load factor of 2. We then calculated the maximum load acting on each wing as 125 N which was the design load used to design the spar. The ultimate load was found as 150% of the design load and was calculated as 187.5 N.

Landing Gear: The team considered a design load factor of 2 to account for the landing shock, vertical drafts & impact loading and landing on only one wheel. We found the design & ultimate loads as 247.212 N and 370.818 N respectively.

10.6.3 Material Selection: We conducted a thorough material trade study factoring in cost, weight, ease of manufacturing and repair. We compared aluminum, titanium and alloy steel for the landing gear & wing spars, selecting aluminum as its yield strength was closest to the design load. We selected balsa & aeroply for the rest of the aircraft components due to their good strength-to weight ratio and the teams experience in working with them.

Material	Mass of Spar (lb.)	Yield Strength (MPa)	Cost Factor
Aluminum 6061	**0.463**	**276**	**0.03**
Titanium 6AL-4V	1.289	880	1
Alloy Steel 4340	1.349	472.3	0.04

Table 17: Spar Material Trade-off

Material	Density	Yield strength (MPa)	Elastic Modulus (GPa)	Shear Strength (MPa)	Shear Modulus (GPa)
Balsa wood	$0.16x10^{-3}$	7(comp)	3.71	3.1	0.23
		14(tensile)			

Aero Ply	$0.35x10^{-3}$	27(comp) 48(tensile)	7.66	6.825	1.78
Aluminum 6061	$2.83x10^{3}$	276	77.34	304	28

Table 18: Properties of Selected Materials

AIRCRAFT COMPONENT	MATERIALS USED
Landing gear/ Spar	Aluminium 6061
Empennage	Balsa, Aero Ply, Ply wood
Fuselage	Aeroply, Bass wood & Balsa
Control surfaces	Balsa wood
Wing	Hard and soft balsa wood, aluminium 6061

Table 19: Materials used in different components of aircraft

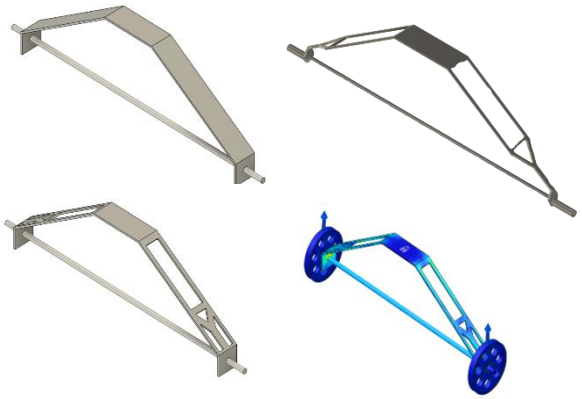

Figure 23: Landing Gear Topology Study & Analysis

10.6.4 Landing Gear Analysis: The team conducted a topology study on our primary landing gear structure to remove material from the non-critical regions of the landing gear, leading to a 30% reduction in weight from our previous design. We applied half the weight of the fully loaded aircraft on each wheel of the landing gear for the analysis from which the maximum stress was found to be 100.4Mpa, resulting in a FoS of 2.74.

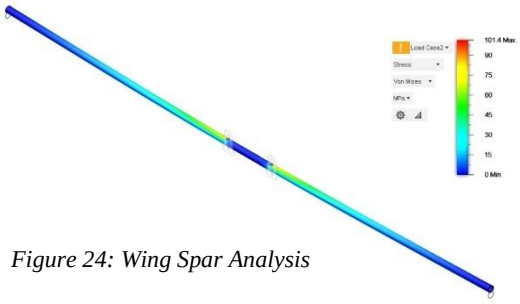

Figure 24: Wing Spar Analysis

10.6.4 Wing Spar Analysis: The team conducted analyses on commercially available spar variants by applying maximum load at the ends of the spar. This load was taken as the lift generated during a 60° bank. The selected spar configuration is 1mm thick with an outer diameter of 0.75” on which the maximum stress was found to be 101.4MPa realizing a FoS of 2.712.

10.6.5 Critical Margins Table:

Component	Yield Strength (MPa)	Safety Factor	Allowable Stress (MPa)	Actual Stress (MPa)	Realized Factor of Safety	Margin of Safety
Wing Spar	276	2	138	101.4	2.712	0.356
Landing Gear	276	2	138	100.4	2.740	0.370

Table 20: Critical Margins Table

11. Manufacturing:

We evaluated various manufacturing processes for each component including the wings, fuselage, tail and landing gear before constructing the aircraft. The manufacturing processes selected represented the best combination of weight, speed of fabrication, ease of repair, team experience with the process, and cost.

11.1 Processes: We employed the following manufacturing processes to ensure accurate fabrication.

Process	Application
Laser cutting	Fuselage cross-sections, airfoil ribs and main landing gear frame
Turning	Side-wing balsa spar
Drilling	All component attachments
CNC machining	Landing gear wheels
CNC bending	Main landing gear
Welding	Landing gear structure
Monokoting	Entire airplane
Adhesion	(Use of cyanoacrylate and epoxy resin) All components
Finishing	All wooden components

Table 21: Manufacturing Processes Employed

11.2 Manufacture of Components: Precision was vital in the fabrication process to avoid deviations from the 2D drawing.

11.2.1 Wing: The airfoils were laser cut and assembled over the aluminum spar. We stuck narrow strips of 2mm balsa on the airfoils to provide a smooth surface during monokoting and provide strength to the airfoils by acting as an I beam. To ensure accurate placement and proper spacing between airfoils, we made marks on the spar placed at the leading edge of the wing and on the aluminum spar.

11.2.2 Fuselage: The cross-sections of the fuselage were laser cut and assembled with stringer beams of dimensions 0.118” X 1”. We stuck the stringer beams to the cross sections using epoxy resin.

11.2.3 Empennage: The airfoils of the horizontal stabilizer were assembled over a 0.394”X0.394” spar

and a 0.118" X 1" spar for those of the vertical stabilizer. Both stabilizers were attached using 2 secondary spars at their trailing edge. The rudder & the elevator had a 0.197" X 0.197" spar supporting all the airfoils.

11.2.4 Landing Gear: For the landing gear, a 1.5" wide aluminum strip of 0.118" thickness was laser cut and then bent on a CNC machine to get the desired shape. Ball bearings were fit on the CNC machined wheels. This wheel assembly was then inserted onto the shaft which in turn was welded to the main frame.

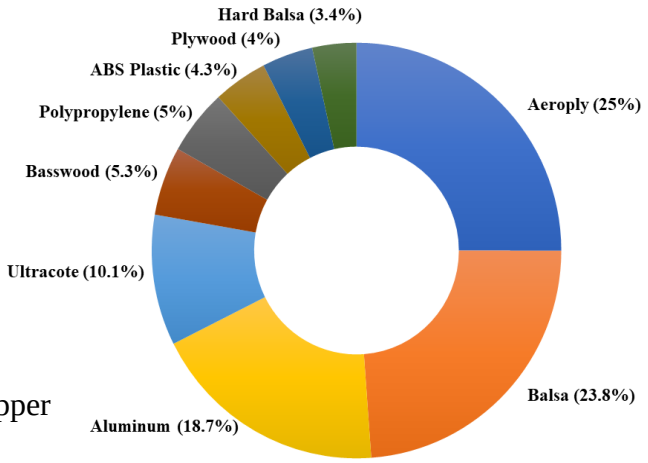

Figure 25: Material wise weight build-up

11.3 Weight Build-up: We constantly monitored the aircraft's weight during the fabrication process to achieve our target empty weight of 0.36. We set an upper weight limit for each component and the CAD design was done accordingly keeping in mind structural integrity. We ensured we did not exceed these limits during the actual fabrication process. Fig 25 shows the weight contribution of each material towards the total empty weight. After a continuously monitored fabrication process, the empty weight of our aircraft (powerplant & electronics included) came up to be 9.52 lb., achieving an empty weight ratio of 0.34, surpassing our initial target.

Total Empty Mass	9.52 lb.	Weight (lb)	Position (in) w.r.t firewall	Moment (lbf.in)
Actual CG	37% of M.A.C			
Motor Assembly & Avionics	Motor & Propeller	1.06	-1.5	-15.60
	Electronics	0.42	8.50	35.02
	Battery	1.5	5.59	82.20
Fuselage	Landing Gear	0.73	29.57	211.69
	Nose Landing Gear	0.44	9.80	42.28
	Fuselage	3.12	38.54	1179.55
Wings	Top Wing	2.07	25.91	526.2
	Bottom Wing	1.26	25.91	320.29
Empennage	Vertical Stabilizer	0.59	67.34	389.75
	Horizontal Stabilizer	0.56	71.24	391.32
Total Moment about Firewall	3162.7			

Table 22: Weight Build-up

11.4 Cost: We fixed a budget of $4500 for the entire project with the money being raised through college funding and contributions from team members. We made a strict budget plan allocating funds for various components & their associated manufacturing processes while accounting for spares and replacements. In the case we exceeded the allocated amount in one category, we made sure to make it up in another by minimizing wastage and judiciously utilizing our funds to keep us within the budget. The unit cost of our aircraft came up to be $1850 and the total cost of the project including registration & cargo shipment came to $3900.

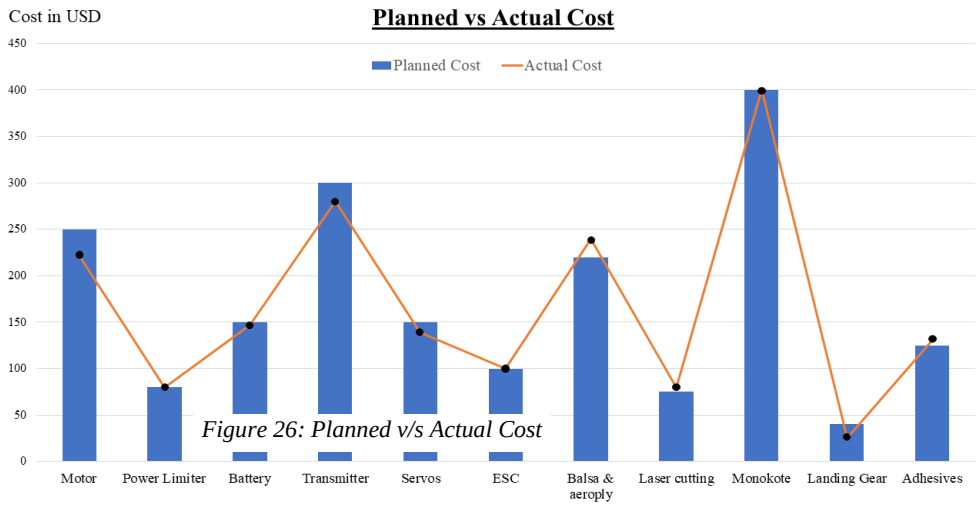

Figure 26: Planned v/s Actual Cost

12. Structural Testing: We conducted structural testing to validate the results of the virtual analysis. The aircraft was first completely assembled before carrying out structural tests. To test the wing strength, we placed weights over the wing simulating an elliptical lift distribution, which they were able to withstand. To test the landing gear, we conducted a drop test where the fully loaded aircraft was dropped from a height of 3 inches. This test proved the endurance of the landing gear. For testing the C.G. of the aircraft, the final aircraft was mounted on a C.G. stand using two supports. This test verified the location of C.G. at 37% M.A.C as desired.

.

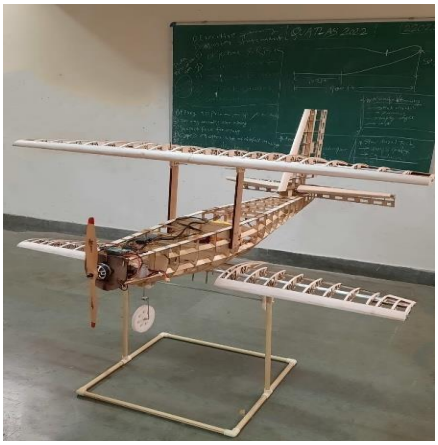

Figure 27: C.G Balance

Figure 28: Wing Testing

13. Flight Score Prediction: We fabricated the airplane such that its empty weight ratio comes up to 0.34, beyond our target of 0.36, thereby allowing us to carry a total payload of 16 lb. Assuming our payload prediction bonus to be 10, the total flight score is predicted to be 122.

14. Conclusion: For this year's aircraft, the team analyzed the scoring equation and emphasized designing an air frame which would obtain the best flight score. We came up with innovative features and solutions in the design to implement our chosen configurations for the aircraft along with designing a new fuselage structure to reduce the empty weight compared to our previous aircrafts. In the process, we had a great learning experience and are confident in our fabrication to make the predicted flight score of 122 a reality and help us win the competition.

15. Formulae:

$$F1.\quad S_g = \frac{1.21 * \frac{W}{S}}{g * \rho_\infty * C_{Lmax} * \frac{T}{W}}$$

$$F2.\quad M_{Hinge} = K * \frac{1}{2} * \rho_\infty * V^2 * Control\ surface\ area * flap\ chord$$

$$F3.\quad \left(\frac{L}{D}\right)_{max} = \sqrt{\frac{1}{4C_{D,o}K}}$$

$$F4.\quad FFS = Final\ Flight\ Score = FS1 + FS2 + FS3 + PPB$$

$$FS = Flight\ Score = 120 * \frac{3*S+W_{payload}}{b+L_{cargo}}$$

$$PPB = Payload\ Prediction\ Bonus = 10 - (A - P)^2$$

$$F5.\quad Margin\ of\ Safety = \frac{Realized\ Factor\ of\ Safety}{Design\ Safety\ factor} - 1$$

16. References:

1	Anderson, John. Fundamentals of Aerodynamics. 5th ed. New York: MC.G.raw-Hill, 2011.
2	Raymer, Daniel P. Airplane Design: A Conceptual Approach. 3rd edition.
3	Anderson, John. Airplane Performance and Design. 2nd ed. Tata MC.G.raw-Hill Edition 2010
4	Robert C. Nelson - Flight stability and automatic control
5	Mohammad H. Sadraey- Airplane Design A Systems Engineering Approach
6	M. S. Ramaiah Institute of Technology (2020), SAE Aero Design Report 2020 (Team Quatlas)
7	M. S. Ramaiah Institute of Technology (2021), SAE Aero Design Report 2021 (Team Quatlas)
8	AIAA 2020 Winning Reports
9	Guerrero, Joel & Sanguineti, Marco & Wittkowski, Kevin. (2019). Variable cant angle winglets for improvement of aircraft flight performance
10	Florida International University. (2015). 2015 SAE Aero Design East Competition

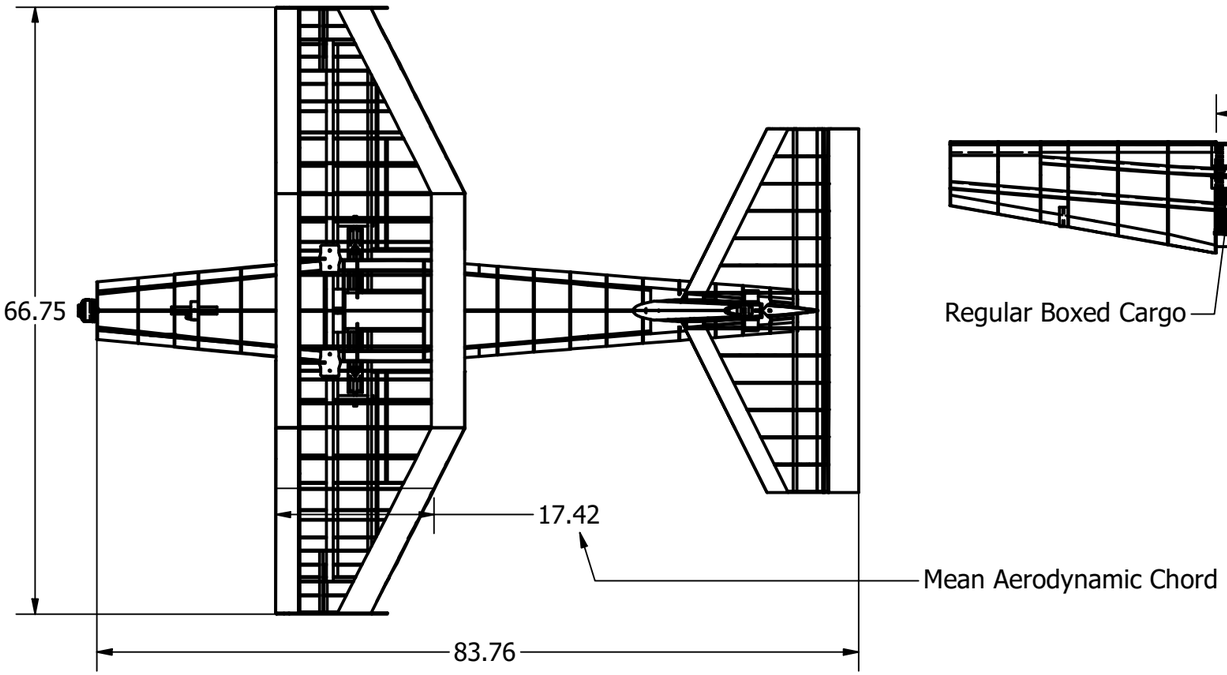

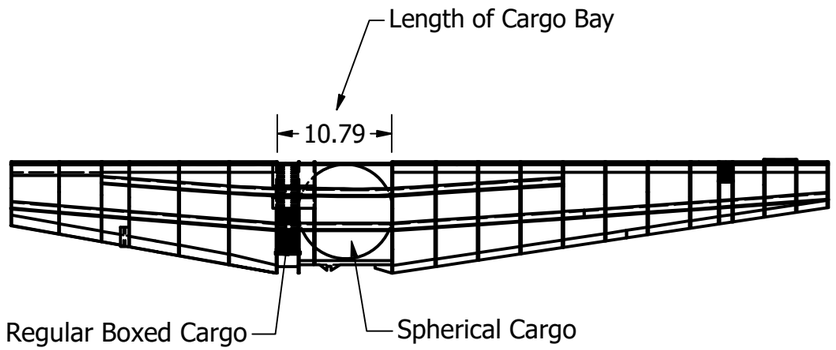

Wingspan	66.75 in
Empty Weight	9.52 lb
Battery Capacity	5200 mAh
Motor Model	KDE 5215XF-330
Motor KV	330 KV
Propeller	Aerostar 21X10
Rudder & Elevator Servo	Hitec HS 225 MG 54 oz-in
Nose gear & Flaperon Servo	Hitec HS 645 MG 107 oz-in

Weight & Balance Information			
Component	Distance from Datum 'A'	Weight	Moment
Motor & Propeller	-1.5 in	1.06 lb	-15.60 lbf.in
Battery	5.59 in	1.5 lb	82.20 lbf.in
Electronics	8.50 in	0.42 lb	35.02 lbf.in
Nose Gear	9.80 in	0.44 lb	42.28 lbf.in
Bottom Wing	25.91 in	1.26 lb	320.29 lbf.in
Top Wing	25.91 in	2.07 lb	526.20 lbf.in
Payload	28.55 in	8.38 lb	2347.04 lbf.in
Landing Gear	29.57 in	0.73 lb	211.69 lbf.in
Fuselage	38.54 in	3.12 lb	1179.55 lbf.in
Vertical Stabilizer	67.34 in	0.59 lb	389.75 lbf.in
Horizontal Stabilizer	71.24 in	0.56 lb	391.32 lbf.in

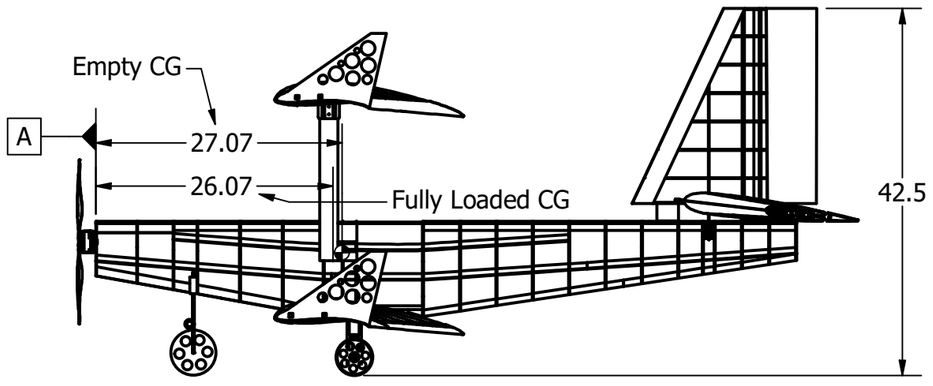

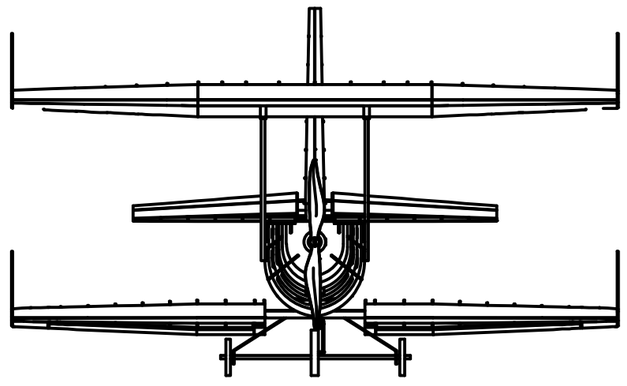

Empty Stability Margin: 10.75% of M.A.C

Fully Loaded Stability Margin: 10% of M.A.C

All Dimensions in Inches

DRAWN	Partha Meravanige
DATE	25 Feb 2022
QA	
MFG	
APPROVED	
SAE Aero Design West 2022	

M. S. Ramaiah Institute of Technology

Team Quatlas - 012

SIZE		DWG NO	REV
B		1	1
SCALE 0.06		SHEET 1 OF 1	

17. Appendix:

The explanation for the payload prediction curve is mentioned in section 10.4 of the report.